Nonuniform ocean acidification and attenuation of the ocean carbon sink

Andrea J. Fassbender[1] (ID), **Christopher L. Sabine[2]** (ID), **and Hilary I. Palevsky[3]** (ID)

[1]Monterey Bay Aquarium Research Institute, Moss Landing, California, USA, [2]Pacific Marine Environmental Laboratory, National Oceanic and Atmospheric Administration, Seattle, Washington, USA, [3]Woods Hole Oceanographic Institution, Woods Hole, Massachusetts, USA

Abstract Surface ocean carbon chemistry is changing rapidly. Partial pressures of carbon dioxide gas (pCO_2) are rising, pH levels are declining, and the ocean's buffer capacity is eroding. Regional differences in short-term pH trends primarily have been attributed to physical and biological processes; however, heterogeneous seawater carbonate chemistry may also be playing an important role. Here we use Surface Ocean CO_2 Atlas Version 4 data to develop 12 month gridded climatologies of carbonate system variables and explore the coherent spatial patterns of ocean acidification and attenuation in the ocean carbon sink caused by rising atmospheric pCO_2. High-latitude regions exhibit the highest pH and buffer capacity sensitivities to pCO_2 increases, while the equatorial Pacific is uniquely insensitive due to a newly defined aqueous CO_2 concentration effect. Importantly, dissimilar regional pH trends do not necessarily equate to dissimilar acidity ($[H^+]$) trends, indicating that $[H^+]$ is a more useful metric of acidification.

1. Introduction

A well-documented feature of the modern anthropogenic era is the rising partial pressure of carbon dioxide gas (pCO_2) in the atmosphere primarily due to fossil fuel burning [*Ciais et al.*, 2013]. In most ocean regions, trends in sea surface pCO_2 roughly parallel trends in atmospheric pCO_2 as the ocean works to maintain air-sea equilibrium [*Takahashi et al.*, 2009; *Bates et al.*, 2014; *Sutton et al.*, 2014]. Due to the tight negative correlation between pCO_2 and pH [*Caldeira and Wickett*, 2003; *Doney et al.*, 2009], sustained pH declines associated with anthropogenic carbon dioxide (CO_2) accumulation in the surface ocean (and its interior) have been termed ocean acidification, as lowering pH values are synonymous with rising acidity. Concerns about the stability of ocean carbon uptake and the consequences for transient and equilibrium climate [*Archer et al.*, 1998], as well as the impacts on marine organisms and ecosystems [*Fabry et al.*, 2008; *Guinotte and Fabry*, 2008; *Doney et al.*, 2009], have led to significant advancements in carbon cycle observing, synthesis, and simulation efforts [*Le Quéré et al.*, 2015; *Bakker et al.*, 2016; *Landschützer et al.*, 2016; *Olsen et al.*, 2016; *Talley et al.*, 2016]. Through these achievements, scientists are now beginning to characterize trends in changing surface ocean chemistry using ocean time series [*Bates et al.*, 2014; *Sutton et al.*, 2014], data synthesis [*Lenton et al.*, 2012; *Fay and McKinley*, 2013; *Lauvset et al.*, 2015; *Munro et al.*, 2015], and climate model [*Lovenduski et al.*, 2015] approaches. Evidence of unique, short-term trends in seawater chemistry has been identified in various ocean regions due to heterogeneity in processes other than anthropogenic CO_2 accumulation that influence sea surface pCO_2 expression and air-sea CO_2 exchange. These processes include ocean circulation and mixing, regional freshwater cycles, and biological processes. While the anthropogenic carbon signal primarily imprints on top of local dynamics, variability or secular changes in these processes due to natural or anthropogenic effects can attenuate or amplify the anthropogenic CO_2 forcing [*Lenton et al.*, 2012], causing a range of surface ocean pCO_2 trends and time scales over which the anthropogenic trend will emerge from natural variations [*McKinley et al.*, 2016, 2017].

In addition to process-driven pCO_2 variability in the surface ocean, there are important thermodynamic effects resulting from anthropogenic carbon accumulation that alter rates of chemical change in seawater. Many of these effects have been mentioned in the literature; however, to the best of our knowledge, they have not yet been synthesized or explored in a comprehensive manner in regard to ocean acidification. Here we build upon theoretical constructs identified by prior investigators and evaluate coherent spatial patterns of thermodynamically driven changes in surface ocean carbonate chemistry.

2. Background Theory and New Expansions

2.1. Conceptual Construct

The ocean and atmosphere are constantly trying to reach equilibrium between their respective pCO_2 values, where seawater pCO_2 is related to the aqueous CO_2 concentration ($[CO_{2\ aq}]$) through Henry's law via the temperature-, salinity-, and pressure-dependent CO_2 solubility constant (K_H) [*Weiss*, 1974].

$$pCO_2 = K_H \times \left[CO_{2\ aq}\right] \tag{1}$$

In seawater, $CO_{2\ aq}$ can molecularly transform by reacting with water to create carbonic acid (H_2CO_3), which often loses a hydrogen ion (H^+) or two to become bicarbonate (HCO_3^-) or carbonate (CO_3^{2-}) ion, respectively [*Millero*, 2007].

$$CO_{2\ aq} + H_2O \leftrightarrow H_2CO_3 \tag{2}$$

$$H_2CO_3 \leftrightarrow HCO_3^- + H^+ \tag{3}$$

$$HCO_3^- \leftrightarrow CO_3^{2-} + H^+ \tag{4}$$

Dissolved inorganic carbon (DIC) represents the sum of all molecular derivatives ($CO_{2\ aq}$, H_2CO_3, HCO_3^-, and CO_3^{2-}) resulting from the dissolution and subsequent hydration of CO_2 gas in water. The transformation of $CO_{2\ aq}$ into alternative molecular forms maintains favorable conditions for more CO_2 gas to dissolve. This gives the ocean a large capacity to absorb and store carbon from the atmosphere, while the deprotonation of carbonic acid (3) tightly links the process to ocean acidification.

Revelle and Suess [1957] estimated the average lifetime of a CO_2 molecule in the atmosphere before being absorbed by the sea and introduced a dimensionless parameter to account for the "peculiar buffer mechanism of sea water" (p. 24). This parameter was later cemented in the literature by *Sundquist et al.* [1979], *Broecker et al.* [1979], and *Takahashi et al.* [1980] as the Revelle factor (RF), which is defined as the fractional change in seawater pCO_2 divided by the fractional change in DIC for a given perturbation.

$$RF = \frac{\partial pCO_2 / pCO_2}{\partial DIC / DIC} \tag{5}$$

Since *Revelle and Suess* [1957] first introduced the concept of an oceanic carbon buffer, several methods have been used to calculate [*Broecker et al.*, 1979; *Takahashi et al.*, 1980] and estimate [*Sarmiento and Gruber*, 2006] RF.

Low RF values indicate that a smaller relative change in pCO_2 is required to elicit a change in DIC because it is easier to move $CO_{2\ aq}$ through the equilibrium reactions to form other molecular derivatives so that more CO_2 gas can enter the ocean. Thus, in the context of anthropogenic carbon uptake, more efficient transfer of carbon from the atmosphere to ocean occurs in regions with low RF values [*Sabine et al.*, 2004]. This concept is analogous to that of buffering, which is the reduction in impact of a chemical change through molecular rearrangement. As a result, a common moniker for the Revelle factor, which describes the efficiency of molecular rearrangement, is the ocean buffer factor, where high buffering capacities are equivalent to low RFs.

2.2. RF Nonlinearity and Sensitivities

A well-known characteristic of the RF response to increasing DIC concentrations is the asymmetric bell-shaped curve that peaks close to where the concentration of DIC equals that of total alkalinity (TA), declining thereafter [*Takahashi et al.*, 1980; *Frankignoulle*, 1994; *Egleston et al.*, 2010]. Figure 1a shows this behavior for a range of fixed TA values across which the DIC concentration is varied. The shape of the RF
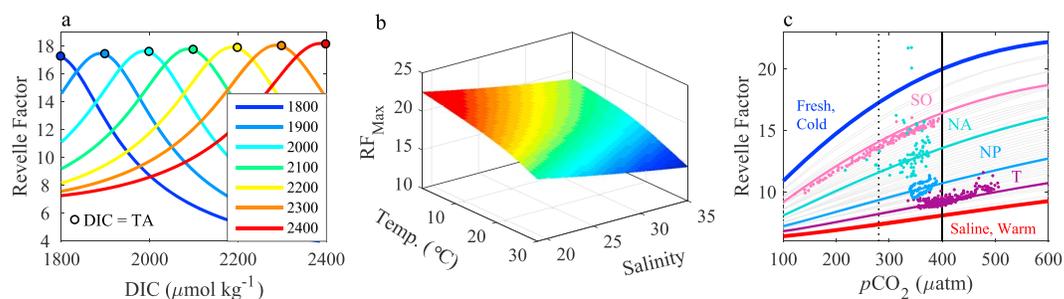
Figure 1. (a) Revelle factor (RF) versus DIC for surface waters at 10°C, salinity 34, and the fixed TA concentrations noted in the legend. Circles show DIC = TA. (b) RF_{max} dependency on temperature and salinity for waters with 2200 µmol kg^{-1} TA and pCO$_2$ ranging from 25 to 1400 µatm. (c) RF versus pCO$_2$ for the same conditions presented in Figure 1b (limited to the 100 to 600 µatm pCO$_2$ range) where gray lines show different temperature and salinity conditions with the fresh (19), cold (2°C) and saline (35), warm (30°C) curves highlighted in blue and red, respectively. Overlain are labeled curves that were computed using median values of annual mean SSS, SST, and TA from grids within the Southern Ocean (SO), North Atlantic (NA), North Pacific (NP), and tropics (T) sectors described in the text while varying input pCO$_2$ across the x axis range. Annual mean pCO$_2$ and RF values from the grids within each sector are plotted. Dotted and solid vertical black lines show preindustrial (280 µatm) and modern (400 µatm) atmospheric pCO$_2$ levels, respectively.

curve has been well described previously by *Takahashi et al.* [1980] and *Egleston et al.* [2010], where the buffer minimum (RF maximum) emerges halfway in between the two carbonate system pK_a values (where p = $-\log_{10}$; K_a = acid dissociation constants for equations (3) and (4)), near a pH of ~7.5. Farther from this point in either direction, buffering increases and RF values decline. This characteristic nonlinearity is significant because it indicates an amplification of the ocean's response to anthropogenic carbon accumulation through a nonlinear decrease in ocean buffer capacity as RF approaches its maximum (RF_{max}) [*Takahashi et al.*, 1980; *Yi et al.*, 2001; *Riebesell et al.*, 2009; *Egleston et al.*, 2010; *Omta et al.*, 2010]. In the modern open ocean, RF values have not yet reached RF_{max} and are increasing in response to carbon accumulation. RF_{max} is not significantly influenced by TA as nearly all curves in Figure 1a display similar maximums (mean ± 1σ: 17.7 ± 0.3); however, it is highly sensitive to temperature [*Broecker et al.*, 1979; *Sundquist et al.*, 1979] and salinity, increasing nonlinearly as both decline (Figure 1b).

While interesting, these RF characteristics are only relevant to anthropogenic climate change if the modern ocean will be influenced by their effects. Figure 1c shows the relationships between RF and pCO$_2$ for the same seawater conditions in Figure 1b (see caption). Additionally, curves representing four unique ocean regions are shown, which were estimated using 12 month climatologies derived from Version 4 of the Surface Ocean CO$_2$ Atlas (SOCAT-V4) that will be described in detail in the subsequent section. These ocean regions were selected to broadly represent a range of chemical domains, including the Southern Ocean (south of 65°S), the subtropical North Pacific Ocean (30°N–40°N, 130°W–150°E), the subpolar North Atlantic Ocean (55°N–68°N, 80°E–0°), and the tropics (6°S–6°N). The curves were developed by perturbing pCO$_2$ around the median chemistry within each domain. Figure 1c indicates that RF grows more rapidly in fresh, cold water regions, which exhibit the highest RF_{max} values, and more slowly in saline, warm water regions in response to rising pCO$_2$. This not only makes the low latitudes more efficient at anthropogenic carbon uptake due to their naturally low RF values [*Sabine et al.*, 2004] but also indicates that the latitudinal gradient in buffer capacity will grow as pCO$_2$ rises. Additionally, Figure 1c shows that $\partial RF\, \partial p CO_2^{-1}$ is presently declining with added pCO$_2$, an effect that is more pronounced in fresher, colder waters. Thus, RF values in the high latitudes may become more homogeneous over time as pCO$_2$ rises.

Although nonlinear attenuation in the ocean buffer capacity [*Takahashi et al.*, 1980] and its relation to global climate [*Yi et al.*, 2001] has long been recognized, spatial heterogeneity in the evolution of RF has important implications for interpreting ocean chemistry changes across different chemical domains. Prior investigators have touched on this topic [*Orr*, 2011; *Bates et al.*, 2014; *Lauvset et al.*, 2015]; however, it has not previously been explored comprehensively from a global observational perspective. Having laid out pertinent RF characteristics of the modern ocean, we will now evaluate the implications of spatially nonuniform RF growth with respect to ocean acidification.

3. Methodology

3.1. Monthly Climatologies of Surface Ocean Carbonate Chemistry

To evaluate spatial and temporal variability in RF, as well as other carbonate system parameters, we rely on CO_2 fugacity (fCO_2) data from Version 4 of the Surface Ocean CO_2 Atlas (SOCAT-V4: http://www.socat.info/) [*Pfeil et al.*, 2013; *Bakker et al.*, 2016], where fCO_2 is much like pCO_2 but takes into account the nonideal nature of the gas. SOCAT-V4 fCO_2 data with WOCE quality control flags of 2 (good) and SOCAT metadata flags A through D were downloaded along with the accompanying sea surface salinity (SSS) and sea surface temperature (SST) observations. By applying these quality control flags, the fCO_2 data used in this analysis have uncertainties of 5 μatm or less [*Bakker et al.*, 2016]. This data set includes ~18.5 million quality-controlled fCO_2 observations collected from 1957 to 2015, though not uniformly distributed in time or space. Due to the decadal spread in observations, a sea surface anthropogenic pCO_2 trend of 1.5 μatm yr^{-1} was used to normalize the fCO_2 observations to the reference year 2010, following *Takahashi et al.* [2009, 2014]. Use of a pCO_2 trend to normalize the fCO_2 observations introduces an uncertainty that is negligible ($<$0.5 μtam) relative to the measurement uncertainty of 5 μtam.

In order to constrain the inorganic carbon chemistry of seawater, a second carbonate system parameter is required [*Dickson and Riley*, 1978; *Millero*, 2007]. TA was estimated from SOCAT-V4 SSS and SST observations using equation (8) of the Locally Interpolated Alkalinity Regression suite of algorithms [*Carter et al.*, 2016] and combined with SSS, SST, and the 2010 normalized fCO_2 observations to calculate DIC, pH, RF, and pCO_2 with the MATLAB program CO2SYS version 1.1 [*Lewis and Wallace*, 1998; *van Heuven et al.*, 2011]. For all CO2SYS calculations the equilibrium constants of *Lueker et al.* [2000] and *Dickson* [1990] and the boron-to-chlorinity ratio of *Uppström* [1974] (following the recommendation of *Orr et al.* [2015]) were applied. Observations collected from the equatorial Pacific between 6°N and 6°S and 130°E and 80°W during El Niño years (Table S1 in the supporting information; $n = 2,521$) were omitted from the analysis following the approach of *Takahashi et al.* [2009, 2014]. The remaining data were gridded to a 3° × 3° global scale, and monthly averages were made for each parameter before averaging across years to create a single 12 month climatology for each grid cell. Uncertainties inherent to the methodology are described in the supporting information Text S1, and Figure S2 shows the number of unique months represented in fCO_2 climatologies for each grid cell.

3.2. Validation Climatologies From Time Series Sites

Data from select time series locations where the seasonal cycle of carbonate system variables has been well resolved were used to validate the gridded SOCAT-V4 climatologies. These sites include the Kuroshio Extension Observatory (KEO; 32.3°N, 144.5°E; https://data.nodc.noaa.gov/cgi-bin/iso?id=gov.noaa.nodc:0100071; *Fassbender et al.*, 2017), Ocean Station Papa (OSP; 50°N, 145°W; https://data.nodc.noaa.gov/cgi-bin/iso?id=gov.noaa.nodc:0100074; *Fassbender et al.*, 2016), Bermuda Atlantic Time Series Study (BATS; 32°N, 64°W; http://bats.bios.edu/), Hawaii Ocean Time Series (HOT; 22.75°N, 158°W; http://hahana.soest.hawaii.edu/hot/hot-dogs/), Irminger Sea (64.3°N, 28°W; http://cdiac.ornl.gov/ftp/oceans/CARINA/Irminger Sea/IrmingerSea_V2/), Iceland Sea (68°N, 12.66°W; http://cdiac.ornl.gov/ftp/oceans/CARINA/IcelandSea//IcelandSea_V2/), and two regions in the Southern Ocean (SO; 57°S, 64°W and 61.5°S, 62°W; *Munro et al.*, 2015) north and south of the Antarctic Polar Front in Drake Passage. Measured, and for some sites estimated, carbonate system parameters were used to calculate other parameters of interest. Details about the development of these climatologies can be found in the supporting information Text S2.

4. Results and Discussion

4.1. Regional Variability and Trends in the Modern Ocean

Annual mean RF values determined from the SOCAT-V4 climatologies are shown in Figure 2a. The results are similar to *Sabine et al.* [2004] showing high RF values near the poles that decline toward the equator, with slightly elevated values in the eastern equatorial Pacific. Figures 2c and 2e show the annual mean distributions for DIC normalized to salinity 35 (nDIC) and pH, respectively. DIC is salinity normalized to more easily compare carbon characteristics from neighboring regions that may experience different net precipitation or evaporation levels and to compare our results with prior studies. nDIC exhibits a similar spatial pattern to RF, while pH displays a unique pattern with some of the highest pH values found in the polar regions
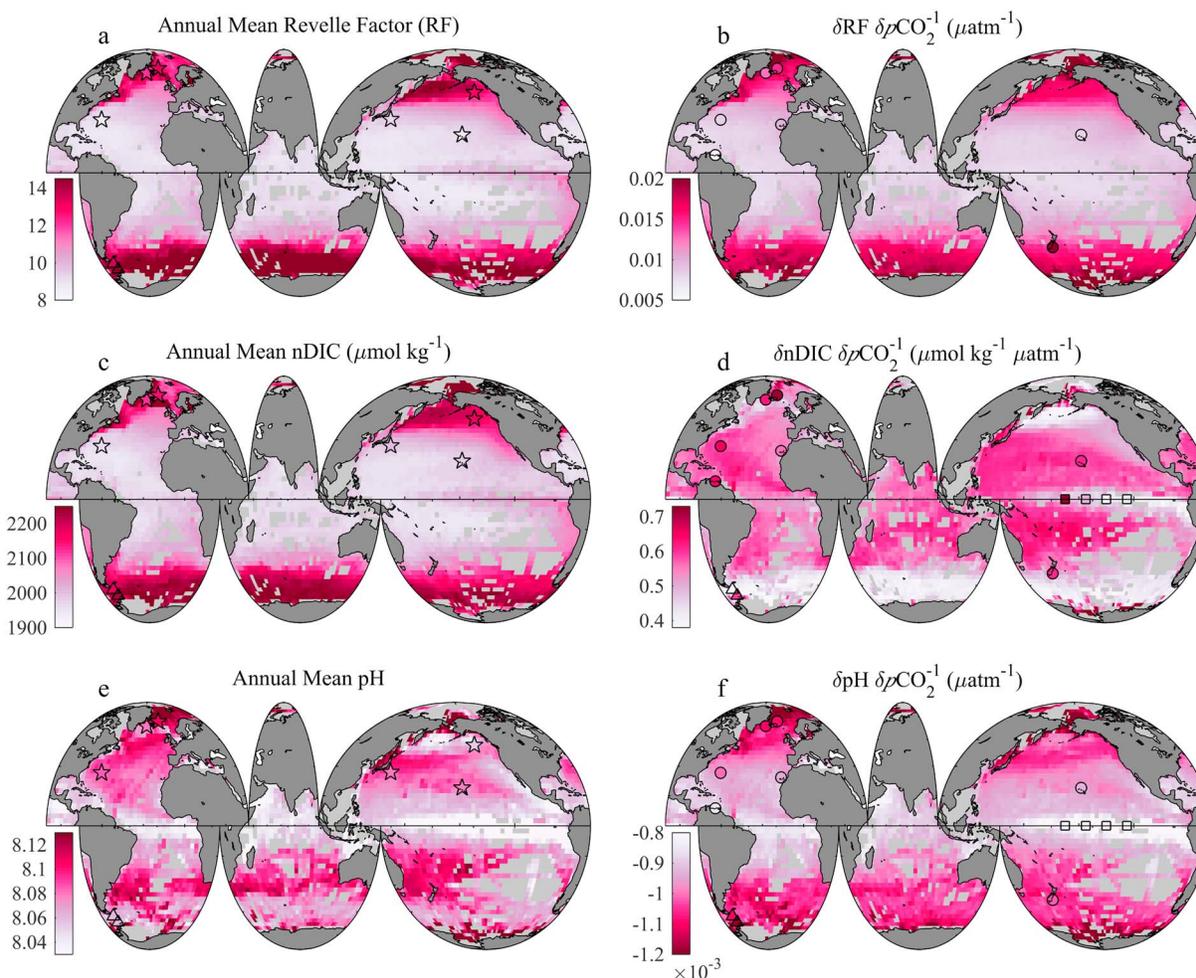
Figure 2. Annual mean (a) RF (c) DIC normalized to salinity 35 (nDIC), and (e) pH. Stars in Figures 2a, 2c, and 2e represent independent estimates from six time series locations, including KEO, OSP, BATS, HOT, Irminger Sea, and Iceland Sea. Triangles represent estimates from two regions in the Southern Ocean from *Munro et al.* [2015]. Rates of change relative to $p\text{CO}_2$ for (b) RF, (d) nDIC, and (f) pH derived from linear $p\text{CO}_2$ perturbations on climatological annual mean values. Circles, squares, and triangles in Figures 2b, 2d, and 2e represent independent $p\text{CO}_2$-normalized estimates of RF, nDIC, and pH trends from *Bates et al.* [2014], *Sutton et al.* [2014], and *Munro et al.* [2015], respectively. Trends from these studies include observations from El Niño years.

and subtropics, similar to the findings of *Takahashi et al.* [2014]. We also find that the lowest pH values occur in the equatorial Pacific where old waters with high DIC content are upwelled to the surface. Annual mean RF, nDIC, and pH values from select time series sites (section 3.2) are also shown in Figures 2a, 2c, and 2e. Agreement between the time series and SOCAT-V4 climatologies (Table S2 and Figure S1) indicates that the gridded values accurately represent carbonate chemistry conditions across a range of latitudes and ocean realms.

To evaluate the modern sensitivity of these parameters to ocean CO_2 uptake, we used the SOCAT-V4 climatology annual mean SST, SSS, DIC, and $p\text{CO}_2$ values in each grid to calculate changes to RF, nDIC, and pH while varying the input $p\text{CO}_2$ values by ±4 μatm using CO2SYS. This simulates approximately 4 years of modern atmospheric $p\text{CO}_2$ growth at a rate of 2 μatm yr^{-1}. The output RF, nDIC, and pH values were then regressed against the input $p\text{CO}_2$ values to determine the slope or rate of change. The results are shown in Figures 2b, 2d, and 2f. Additionally, recent trend estimates for RF, nDIC, and pH from *Bates et al.* [2014], *Sutton et al.* [2014], and *Munro et al.* [2015] were normalized by the associated $p\text{CO}_2$ trends from each study and are shown for comparison purposes. Agreement between the chemical perturbation results and time series data in Figures 2b, 2d, and 2f (Table S3) indicates that chemical thermodynamics can explain most
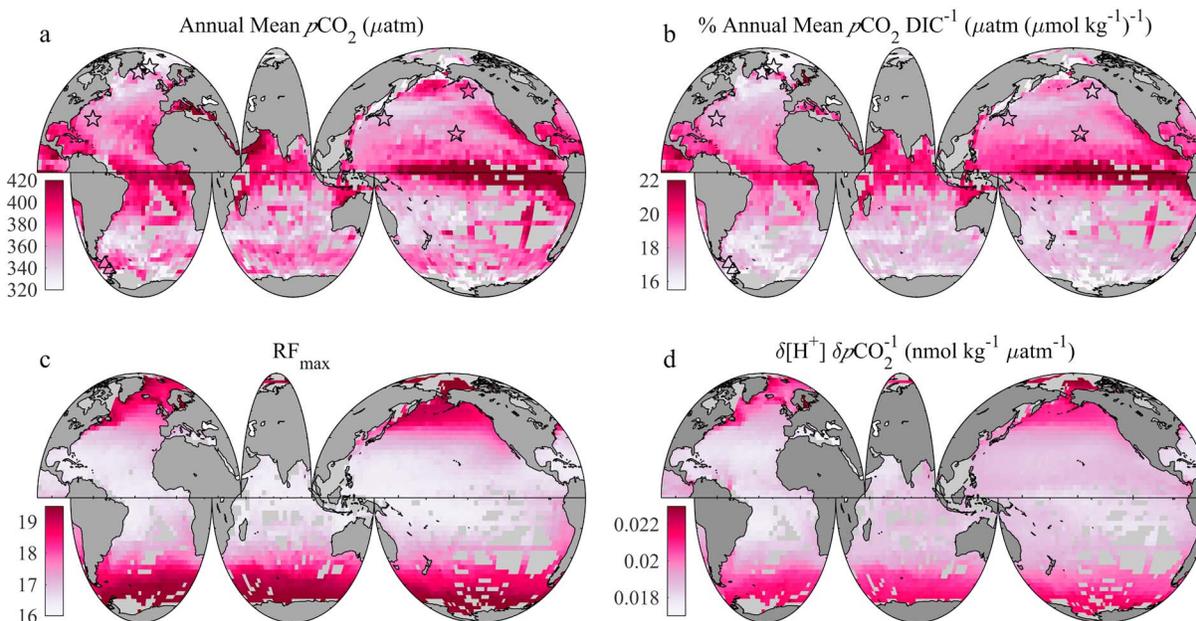
Figure 3. Annual mean (a) pCO_2 and (b) $pCO_2 \, DIC^{-1}$. Stars represent independent estimates from six time series locations, including KEO, OSP, BATS, HOT, Irminger Sea, and Iceland Sea. Triangles represent estimates from two regions in the Southern Ocean from *Munro et al.* [2015]. (c) RF_{max}. (d) $\partial[H^+] \, \partial pCO_2^{-1}$ derived from linear pCO_2 perturbations as in Figure 2.

of the spatial variability in observed trends. Areas with larger disagreement (i.e., equatorial Pacific $\partial nDIC$ ∂pCO_2^{-1}) suggest that processes other than pure thermodynamics are relevant.

RF values increase most rapidly with added pCO_2 in high-latitude regions where RF values are already high (Figure 2b), matching the expectation of higher $\partial RF \, \partial pCO_2^{-1}$ in colder, fresher waters (Figure 1c). Importantly, locations with similar RF values can express different $\partial RF \, \partial pCO_2^{-1}$ and vice versa. Spatial variability in the annual mean RF (Figure 2a) reflects different regional efficiencies of ocean carbon uptake [*Sabine et al.*, 2004; *Egleston et al.*, 2010], which is clearly displayed in Figure 2d. As expected, the change in nDIC per 1 μatm pCO_2 increase ($\partial nDIC \, \partial pCO_2^{-1}$) shows a nearly opposite pattern as $\partial RF \, \partial pCO_2^{-1}$, with larger DIC changes in the tropics and lower DIC changes near the poles. Interestingly, $\partial nDIC \, \partial pCO_2^{-1}$ is also very low in the eastern equatorial Pacific even though nDIC and RF values in this region are similar to those throughout the tropics and much lower than those in the high latitudes. Why is this? $\partial nDIC \, \partial pCO_2^{-1}$ is depressed near the equator due to an aqueous CO_2 concentration ($[CO_{2 \, aq}]$) effect. The equatorial upwelling of old, DIC-rich water with low pH (Figure 2e) and high pCO_2 content (Figure 3a) resulting from extensive remineralization of organic matter causes $CO_{2 \, aq}$ to make up a larger fraction of the nDIC pool than in neighboring regions with similar nDIC concentrations. This leads to a higher $pCO_2 \, nDIC^{-1}$ (equation (1) and Figure 3b). So although RF values are similar throughout the tropics, changing nDIC requires a larger magnitude pCO_2 increase in the equatorial Pacific, leading to the observed insensitivity of nDIC to pCO_2 growth along the equator. This exemplifies that waters with nearly identical RF, RF_{max} (Figure 3c), and nDIC values can display dissimilar carbon uptake efficiencies depending on what fraction of the DIC pool is composed of $CO_{2 \, aq}$.

Finally, Figure 2f shows the change in pH per unit increase in pCO_2, with an inverted color scale since more negative $\partial pH \, \partial pCO_2^{-1}$ values indicate larger pH declines. The biggest changes occur near the poles where RF values are highest and waters are poorly buffered. The smallest changes occur in the equatorial Pacific even though the RF values are similar to those in the tropics. This characteristic is also related to the $[CO_{2 \, aq}]$ effect but in a slightly different way. pH is defined as the negative $\log_{10}$ of $[H^+]$, which is strongly correlated with pCO_2. Thus, pCO_2 increases lead to associated $[H^+]$ increases and pH declines across all ocean locations. However, the change in $[H^+]$ resulting from a given pCO_2 increase is nonuniform and is a function of the temperature- and salinity-dependent carbonate system equilibrium constants as well as the local buffer capacity, which makes $\partial[H^+] \, \partial pCO_2^{-1}$ larger at the poles (Figure 3d). On the other hand, $\partial[H^+] \, \partial pCO_2^{-1}$ is

fairly uniform across the tropics and subtropics. Why then is ∂pH ∂pCO$_2$$^{-1}$ lowest in the equatorial Pacific? This is due to variability in the background [H$^+$], or pH, since the same [H$^+$] change will translate to different pH changes across the pH scale. In the equatorial Pacific where pH values are low (Figure 2e), the pH change imposed by a given [H$^+$] change will be smaller than in regions where the background pH is higher. For example, a 2.3 nmol kg^{-1} increase in [H$^+$] would cause waters with background pH values of 7.9 and 8.2 to decrease to pH values of 7.83 and 8.07, respectively. This means that the same [H$^+$] change caused a 0.07 unit decline in waters with a starting pH of 7.9 and a 0.14 unit decline for waters with a starting pH of 8.2. Thus, the [CO$_2$ $_{aq}$] effect coupled with the logarithmic nature of the pH scale yields the lowest ∂pH ∂pCO$_2$$^{-1}$ values in the eastern equatorial Pacific.

In regard to ocean acidification, biological organisms respond to [H$^+$] rather than pH [e.g., *Taylor et al.*, 2011; *Jokiel*, 2016]; however, pH is often reported because it is a convenient scale to express large [H$^+$] changes. Despite being common practice, comparing pH trends from ocean regions with different annual mean pH is not well suited to the evaluation of regional changes in ocean acidity and can be misleading (Figure S4). [H$^+$] is a more useful parameter since trends in acidity can be directly compared across ocean regions. At present, many pH trends derived from time series sites are statistically indistinguishable [*Bates et al.*, 2014], yet the associated [H$^+$] trends may vary more significantly (e.g., Figures 2f and 3d). Further, regions with dissimilar pH trends may actually exhibit the same [H$^+$] trends over time. [H$^+$] will therefore be a more robust environmental indicator than pH for assessing spatial patterns of ocean acidification.

To summarize, spatial variability in the RF sensitivity to pCO$_2$ results in different rates of carbonate chemistry change throughout the ocean as sea surface pCO$_2$ increases (assuming all else constant). In particular, RF values rise fastest in regions that have high RF$_{max}$ values, namely the high latitudes. Observed trends in surface ocean carbonate chemistry from time series sites [*Bates et al.*, 2014; *Sutton et al.*, 2014; *Munro et al.*, 2015] display a large-scale pattern consistent with the modern thermodynamic response (Figures 2b, 2d, and 2f). However, regional changes in fresh water cycles, biogeochemistry, and circulation have also been identified as contributing factors [*Bates et al.*, 2014; *Sutton et al.*, 2014; *Munro et al.*, 2015]. Importantly, different rates of DIC accumulation (∂nDIC ∂pCO$_2$$^{-1}$) and pH decline ($\partial$pH ∂pCO$_2$$^{-1}$) can occur in regions with identical RF and RF$_{max}$ values that experience the same increase in seawater pCO$_2$. This indicates that the carbonate system response to accumulating anthropogenic carbon cannot be discerned from RF alone and depends on other factors including the background pCO$_2$ DIC^{-1}, pH, and RF$_{max}$. Finally, comparing trends in pH can be misleading when trying to understand rates and spatial patterns of ocean acidification. By using [H$^+$] trends, these challenges can be avoided.

4.2. Consideration of Long-Term Changes in the Mean State

In addition to modern chemical sensitivities to rising pCO$_2$, it is important to consider spatial heterogeneity in how carbonate chemistry will be altered over longer time periods. The highest ∂RF ∂pCO$_2$$^{-1}$ values are found in regions with elevated R$_{max}$ values, which are near the poles where waters are colder and fresher (Figures 1c, 2b, and 3c). As a result, the addition of anthropogenic carbon is causing the polar oceans to more rapidly approach their minimum buffer capacities. As the buffer capacity declines, sea surface pCO$_2$ may rise more rapidly over time [e.g., *Thomas et al.*, 2007], assuming a constant atmospheric pCO$_2$ growth rate, as it becomes harder to move CO$_2$ through the equilibrium reactions (i.e., Le Chatelier's principle). This will lead to faster [H$^+$] increases and reduced (enhanced) CO$_2$ sink (source) strengths as the air-sea disequilibrium is eroded (grows). Thus, ocean acidification may accelerate in polar regions where high RF values continue to increase with added anthropogenic carbon. The lower latitudes, by contrast, are much farther from RF$_{max}$, and ∂RF ∂pCO$_2$$^{-1}$ values are much lower. While it has long been recognized that the impacts of ocean acidification may emerge first in the polar regions due to naturally elevated DIC content in these waters [*Orr et al.*, 2005], the thermodynamic expectation for more rapid rates of ocean acidification (Figure 3d) in these areas [*Orr*, 2011] is not yet widely acknowledged. Importantly, the most rapid RF changes in response to rising sea surface pCO$_2$ have already occurred (Figure 1c), indicating slower rates of attenuation in the ocean carbon sink per unit pCO$_2$ increase—though the temporal evolution of seawater chemistry ultimately depends on the atmospheric pCO$_2$ growth rate.

Another important implication of spatial heterogeneity in ocean carbon uptake is that the more rapid accumulation of anthropogenic carbon in surface waters of the tropics relative to the temperate and high

latitudes (Figure 2d) will reduce the sea surface DIC gradient between regions. Transport of subtropical waters poleward in western boundary currents (WBC) will still result in carbon uptake due to increased pCO$_2$ solubility upon cooling; however, the smaller DIC difference between transported and resident waters will mean that less carbon uptake has to occur in the transported waters in order to reach the equilibrium DIC of the higher latitude [*Völker et al.*, 2002]. As a result, less anthropogenic carbon will be taken up in WBC regions as the sea-air pCO$_2$ difference is eroded over time. This is relevant because WBC regions are hubs of anthropogenic carbon sequestration due to the formation and subsequent dispersal of mode waters into the ocean interior [*Sabine et al.*, 2004; *Levine et al.*, 2011; *Bates*, 2012; *Iudicone et al.*, 2016]. While *Völker et al.* [2002] have explored this phenomenon in the North Atlantic Ocean, further evaluations may be warranted in the context of accelerating degradation of the latitudinal DIC gradient, which may cause surface ocean carbonate chemistry to become more uniform over time.

5. Conclusions

Prior investigators have shown the importance of freshwater balances, physical processes, biogeochemical cycling, wind speed, and large-scale climate variability in regional trends of surface ocean carbonate chemistry [*Lenton et al.*, 2012; *Bates et al.*, 2014; *Sutton et al.*, 2014; *Lauvset et al.*, 2015; *Munro et al.*, 2015]. In addition to these process-driven factors, chemical thermodynamics imparts a coherent signature of change that must be incorporated into the interpretation of ocean carbon cycle responses to anthropogenic forcing. Our findings exemplify the potential for nonuniform ocean acidification and attenuation of the ocean carbon sink as the ocean keeps pace with rising atmospheric pCO$_2$—in the absence of changes to any other processes. Further, regions with identical characteristics (RF, RF$_{max}$, and nDIC) can display dissimilar carbon uptake efficiencies depending on the chemical speciation of the DIC pool. This nuance can lead to significant regional differences in the rate of anthropogenic carbon uptake and pH change as ocean pCO$_2$ grows. Spatial variability in pH trends should be anticipated, and the use of [H$^+$] trends will be necessary to accurately decipher regional differences in ocean acidification. High latitudes are experiencing the most rapid declines in buffer capacity. The acute sensitivity of RF to temperature and salinity equates to significant uncertainty in how polar regions will respond in the coming decades, as warming and freshening have opposing effects on RF. Careful consideration of the thermodynamic drivers of ocean change is necessary to better characterize the sensitivities of ocean carbon uptake and acidification rates to the persistent climb in atmospheric pCO$_2$.

References

Archer, D., H. Kheshgi, and E. Maier-Reimer (1998), Dynamics of fossil fuel CO$_2$ neutralization by marine CaCO$_3$, *Global Biogeochem. Cycles*, *12*(2), 259–276.

Bakker, D. C. E., et al. (2016), A multi-decade record of high-quality fCO$_2$ data in version 3 of the Surface Ocean CO$_2$ Atlas (SOCAT), *Earth Syst. Sci. Data*, *8*(2), 383–413, doi:10.5194/essd-8-383-2016.

Bates, N., Y. Astor, M. Church, K. Currie, J. Dore, M. Gonaález-Dávila, L. Lorenzoni, F. Muller-Karger, J. Olafsson, and M. Santa-Casiano (2014), A time-series view of changing ocean chemistry due to ocean uptake of anthropogenic CO$_2$ and ocean acidification, *Oceanography*, *27*(1), 126–141, doi:10.5670/oceanog.2014.16.

Bates, N. R. (2012), Multi-decadal uptake of carbon dioxide into subtropical mode water of the North Atlantic Ocean, *Biogeosciences*, *9*(7), 2649–2659, doi:10.5194/bg-9-2649-2012.

Broecker, W. S., T. Takahashi, H. J. Simpson, and T.-H. Peng (1979), Fate of fossil fuel carbon dioxide and the global carbon budget, *Science*, *206*(4417), 409–418, doi:10.1126/science.206.4417.409.

Caldeira, K., and M. E. Wickett (2003), Anthropogenic carbon and ocean pH, *Nature*, *425*(September), 365–365, doi:10.1038/425365a.

Carter, B. R., N. L. Williams, A. R. Gray, and R. A. Feely (2016), Locally interpolated alkalinity regression for global alkalinity estimation, *Limnol. Oceanogr. Methods*, *14*(4), 268–277, doi:10.1002/lom3.10087.

Ciais, P., et al. (2013), Carbon and other biogeochemical cycles, in *Climate Change 2013—The Physical Science Basis*, edited by Intergovernmental Panel on Climate Change, pp. 465–570, Cambridge Univ. Press, Cambridge.

Dickson, A. G. (1990), Standard potential of the reaction: AgCl(s) + 1/2H$_2$(g) = Ag(s) + HCl(aq), and the standard acidity constant of the ion HSO$_4^-$ in synthetic sea water from 273.15 to 318.15 K, *J. Chem. Thermodyn.*, *22*, 113–127.

Dickson, A. G., and J. Riley (1978), The effect of analytical error on the evaluation of the components of the aquatic carbon-dioxide system, *Mar. Chem.*, *6*, 77–85, doi:10.1016/0304-4203(78)90008-7.

Doney, S. C., V. J. Fabry, R. A. Feely, and J. A. Kleypas (2009), Ocean acidification: the other CO$_2$ problem., *Ann. Rev. Mar. Sci.*, *1*(1), 169–192, doi:10.1146/annurev.marine.010908.163834.

Egleston, E. S., C. L. Sabine, and F. M. M. Morel (2010), Revelle revisited: Buffer factors that quantify the response of ocean chemistry to changes in DIC and alkalinity, *Global Biogeochem. Cycles*, *24*, GB1002, doi:10.1029/2008GB003407.

Fabry, V. J., B. A. Seibel, R. A. Feely, and J. C. Orr (2008), Impacts of ocean acidification on marine fauna and ecosystem processes, *ICES J. Mar. Sci.*, *65*(3), 414–432, doi:10.1093/icesjms/fsn048.

Fassbender, A. J., C. L. Sabine, and M. F. Cronin (2016), Net community production and calcification from 7 years of NOAA Station Papa Mooring measurements, *Global Biogeochem. Cycles*, *30*, 250–267, doi:10.1002/2015GB005205.

Fassbender, A. J., C. L. Sabine, M. F. Cronin, and A. J. Sutton (2017), Mixed-layer carbon cycling at the Kuroshio extension observatory, *Global Biogeochem. Cycles*, *31*, 272–288, doi:10.1002/2016GB005547.

Fay, A. R., and G. A. McKinley (2013), Global trends in surface ocean pCO_2 from in situ data, *Global Biogeochem. Cycles*, *27*, 541–557, doi:10.1002/gbc.20051.

Frankignoulle, M. (1994), A complete set of buffer factors for acid/base CO_2 system in seawater, *J. Mar. Syst.*, *5*(2), 111–118.

Guinotte, J. M., and V. J. Fabry (2008), Ocean acidification and its potential effects on marine ecosystems, *Ann. N. Y. Acad. Sci.*, *1134*, 320–342, doi:10.1196/annals.1439.013.

Iudicone, D., K. B. Rodgers, Y. Plancherel, O. Aumont, T. Ito, R. M. Key, G. Madec, and M. Ishii (2016), The formation of the ocean's anthropogenic carbon reservoir, *Sci. Rep.*, *6*(1), 35473, doi:10.1038/srep35473.

Jokiel, P. L. (2016), Predicting the impact of ocean acidification on coral reefs: Evaluating the assumptions involved, *ICES J. Mar. Sci. J. du Cons.*, *73*(3), 550–557, doi:10.1093/icesjms/fsv091.

Landschützer, P., N. Gruber, and D. C. E. Bakker (2016), Decadal variations and trends of the global ocean carbon sink, *Global Biogeochem. Cycles*, *30*, 1396–1417, doi:10.1002/2015GB005359.

Lauvset, S. K., N. Gruber, P. Landschützer, A. Olsen, and J. Tjiputra (2015), Trends and drivers in global surface ocean pH over the past 3 decades, *Biogeosciences*, *12*(5), 1285–1298, doi:10.5194/bg-12-1285-2015.

Le Quéré, C., et al. (2015), Global carbon budget 2015, *Earth Syst. Sci. Data*, *7*(2), 349–396, doi:10.5194/essd-7-349-2015.

Lenton, A., N. Metzl, T. Takahashi, M. Kuchinke, R. J. Matear, T. Roy, S. C. Sutherland, C. Sweeney, and B. Tilbrook (2012), The observed evolution of oceanic pCO_2 and its drivers over the last two decades, *Global Biogeochem. Cycles*, *26*, GB2021, doi:10.1029/2011GB004095.

Levine, N. M., S. C. Doney, I. Lima, R. Wanninkhof, N. R. Bates, and R. A. Feely (2011), The impact of the North Atlantic Oscillation on the uptake and accumulation of anthropogenic CO_2 by North Atlantic Ocean mode waters, *Global Biogeochem. Cycles*, *25*, GB3022, doi:10.1029/2010GB003892.

Lewis, E. and D. W. R. Wallace (1998), Program developed for CO_2 system calculations, *Oak Ridge TN*, vol. 4735, Oak Ridge Natl. Lab. Environ. Sci. Div., Oak Ridge, Tenn.

Lovenduski, N. S., M. C. Long, and K. Lindsay (2015), Natural variability in the surface ocean carbonate ion concentration, *Biogeosciences*, *12*(21), 6321–6335, doi:10.5194/bg-12-6321-2015.

Lueker, T. J., A. G. Dickson, and C. D. Keeling (2000), Ocean pCO_2 calculated from dissolved inorganic carbon, alkalinity, and equations for K_1 and K_2: Validation based on laboratory measurements of CO_2 in gas and seawater at equilibrium, *Mar. Chem.*, *70*(1–3), 105–119, doi:10.1016/S0304-4203(00)00022-0.

McKinley, G. A., D. J. Pilcher, A. R. Fay, K. Lindsay, M. C. Long, and N. S. Lovenduski (2016), Timescales for detection of trends in the ocean carbon sink, *Nature*, *530*(7591), 469–472, doi:10.1038/nature16958.

McKinley, G. A., A. R. Fay, N. S. Lovenduski, and D. J. Pilcher (2017), Natural variability and anthropogenic trends in the ocean carbon sink, *Annu. Rev. Mar. Sci.*, *9*(1), 125–150, doi:10.1146/annurev-marine-010816-060529.

Millero, F. J. (2007), The marine inorganic carbon cycle, *Chem. Rev.*, *107*(2), 308–341, doi:10.1021/cr0503557.

Munro, D. R., N. S. Lovenduski, T. Takahashi, B. B. Stephens, T. Newberger, and C. Sweeney (2015), Recent evidence for a strengthening CO_2 sink in the Southern Ocean from carbonate system measurements in the Drake Passage (2002–2015), *Geophys. Res. Lett.*, *42*, 7623–7630, doi:10.1002/2015GL065194.

Olsen, A., et al. (2016), The Global Ocean Data Analysis Project version 2 (GLODAPv2)—An internally consistent data product for the world ocean, *Earth Syst. Sci. Data*, *8*, 297–323, doi:10.5194/essd-8-297-2016.

Omta, A. W., P. Goodwin, and M. J. Follows (2010), Multiple regimes of air-sea carbon partitioning identified from constant-alkalinity buffer factors, *Global Biogeochem. Cycles*, *24*, GB3008, doi:10.1029/2009GB003726.

Orr, J. C. (2011), Recent and future changes in ocean carbonate chemistry, in *Ocean Acidification*, edited by J.-P. Gattuso and L. Hansson, pp. 41–66, Oxford Univ. Press, New York.

Orr, J. C., et al. (2005), Anthropogenic ocean acidification over the twenty-first century and its impact on calcifying organisms, *Nature*, *437*(7059), 681–686, doi:10.1038/nature04095.

Orr, J. C., J.-M. Epitalon, and J.-P. Gattuso (2015), Comparison of ten packages that compute ocean carbonate chemistry, *Biogeosciences*, *12*(5), 1483–1510, doi:10.5194/bg-12-1483-2015.

Pfeil, B., et al. (2013), A uniform, quality controlled Surface Ocean CO_2 Atlas (SOCAT), *Earth Syst. Sci. Data*, *5*(1), 125–143, doi:10.5194/essd-5-125-2013.

Revelle, R., and H. E. Suess (1957), Carbon dioxide exchange between atmosphere and ocean and the question of an increase of atmospheric CO_2 during the past decades, *Tellus*, *9*(1), 18–27, doi:10.1111/j.2153-3490.1957.tb01849.x.

Riebesell, U., A. Körtzinger, and A. Oschlies (2009), Sensitivities of marine carbon fluxes to ocean change, *Proc. Natl. Acad. Sci.*, *106*(49), 20,602–20,609, doi:10.1073/pnas.0813291106.

Sabine, C. L., et al. (2004), The Oceanic Sink for Anthropogenic CO_2, *Science*, *305*(80, 5682), 367–371, doi:10.1126/science.1097403.

Sarmiento, J. L., and N. Gruber (2006), Carbon cycle, in *Ocean Biogeochemical Dynamics*, pp. 318–355, Princeton Univ. Press, N. J.

Sundquist, E. T., L. N. Plummer, and T. M. L. Wigley (1979), Carbon dioxide in the ocean surface: The homogeneous buffer factor, *Science (80-.).*, *204*(4398), 1203–1205, doi:10.1126/science.204.4398.1203.

Sutton, A. J., R. A. Feely, C. L. Sabine, M. J. McPhaden, T. Takahashi, F. P. Chavez, G. Friederich, and J. T. Mathis (2014), Natural variability and anthropogenic change in equatorial Pacific surface ocean pCO_2 and pH, *Global Biogeochem. Cycles*, *28*, 131–145, doi:10.1002/2013GB004679.

Takahashi, T., W. S. Broecker, S. R. Werner, and A. E. Bainbridge (1980), Carbonate chemistry of the surface waters of the worlds ocean, in *Isotope Marine Chemistry*, edited by K. S. Edward D. Goldberg, and Y. Horibe, pp. 291–326, Geochem. Res. Assoc.

Takahashi, T., et al. (2009), Climatological mean and decadal change in surface ocean pCO_2, and net sea-air CO_2, flux over the global oceans, *Deep Sea Res., Part II*, *56*(8–10), 554–577, doi:10.1016/j.dsr2.2008.12.009.

Takahashi, T., S. C. Sutherland, D. W. Chipman, J. G. Goddard, and C. Ho (2014), Climatological distributions of pH, pCO_2, total CO_2, alkalinity, and $CaCO_3$ saturation in the global surface ocean, and temporal changes at selected locations, *Mar. Chem.*, *164*, 95–125, doi:10.1016/j.marchem.2014.06.004.

Talley, L. D., et al. (2016), Changes in ocean heat, carbon content, and ventilation: A review of the first decade of GO-SHIP global repeat hydrography, *Ann. Rev. Mar. Sci.*, *8*(1), annurev-marine-052915-100829, doi:10.1146/annurev-marine-052915-100829.

Taylor, A. R., A. Chrachri, G. Wheeler, H. Goddard, and C. Brownlee (2011), A Voltage-Gated H^+ Channel Underlying pH Homeostasis in Calcifying Coccolithophores, edited by P. G. Falkowski, *PLoS Biol.*, *9*(6), e1001085, doi:10.1371/journal.pbio.1001085.

Thomas, H., et al. (2007), Rapid decline of the CO_2 buffering capacity in the North Sea and implications for the North Atlantic Ocean, *Global Biogeochem. Cycles*, *21*, GB4001, doi:10.1029/2006GB002825.

Uppström, L. R. (1974), The boron/chlorinity ratio of deep-sea water from the Pacific Ocean, *Deep Sea Res., Part II*, *21*, 161–162.

van Heuven, S., D. Pierrot, J. W. B. Rae, E. Lewis, and D. W. R. Wallace (2011), MATLAB program developed for CO_2 system calculations. ORNL/CDIAC-105b., ORNL/CDIAC-105b. Carbon Dioxide Inf. Anal. Center, Oak Ridge Natl. Lab. U.S. Dep. Energy, Oak Ridge, Tenn., doi:10.3334/CDIAC/otg.CO2SYS_MATLAB_v1.1.

Völker, C., D. W. R. Wallace, and D. A. Wolf-Gladrow (2002), On the role of heat fluxes in the uptake of anthropogenic carbon in the North Atlantic, *Global Biogeochem. Cycles*, 16(4), 85-1–85-9, doi:10.1029/2002GB001897.

Weiss, R. (1974), Carbon dioxide in water and seawater: The solubility of a non-ideal gas, *Mar. Chem.*, *2*(3), 203–215, doi:10.1016/0304-4203(74)90015-2.

Yi, C., P. Gong, M. Xu, and Y. Qi (2001), The effects of buffer and temperature feedback on the oceanic uptake of CO_2, *Geophys. Res. Lett.*, *28*(5), 751–754, doi:10.1029/2000GL011569.